Geophys. J. Int. (2004) **156,** 459–466 doi: 10.1111/j.1365-246X.2004.02212.x

FAST TRACK PAPER

Stress-induced temporal variations in seismic anisotropy observed in microseismic data

N. Teanby,[1,*] J.-M. Kendall,[1] R. H. Jones[2] and O. Barkved[3]

[1] *School of Earth Science, University of Leeds, Leeds* LS2 9JT, *UK*
[2] *ABB Offshore Systems Limited, Rosemanowes, Penryn* TR10 9DU, *UK*
[3] *BP-Norge, Godesetdalen* 8, PO Box 197, 4065 *Stavanger, Norway*

Accepted 2003 December 5. Received 2003 December 2; in original form 2003 July 30

SUMMARY

In situ stress monitoring of crustal rocks is desirable as it yields insights into earthquake mechanisms, volcanic eruptions and changes in hydrocarbon reservoirs. Shear wave splitting, induced by stress-controlled cracks in the shallow crust, provides a way to infer this stress. Temporal variations in these observations can be difficult to quantify due to scatter in the data and discontinuous observations. Here we present evidence of temporal variations in shear wave splitting from a continuous time-series with a high occurrence of microseismic events recorded in a borehole. We interpret these observations in terms of stress-controlled cracks and are able to infer changes in stress and, via modelling, suggest the cause of the anisotropy. Possible origins of the temporal variation in per cent anisotropy are tidal or oil-field production processes. Our results suggest that shear wave splitting is a viable probe for inferring changes in crustal stress in cracked rock.

Key words: anisotropy, seismology, stress monitoring, tides.

1 INTRODUCTION

Observations of crack-induced seismic anisotropy provide insights into crustal stress, and its temporal variation yields insight into changes in that stress (Gupta 1973). However, convincing measurements of temporal variations are difficult to obtain because of scatter in the data and non-continuous recording intervals. Here we present observations of anisotropy inferred from microseismic events at the Valhall oil reservoir (North Sea). The data set provides an ideal opportunity for studying stress changes as we have a continuous 56-day time-series with an average of 15 events per day, recorded on an string of six three-component geophones. The area is prone to large stresses—the seafloor has subsided by more than 4 m since production started and borehole breakout is common in this area. Large variations in shear wave splitting, which is arguably the best indicator of anisotropy, are observed and interpreted in terms of stress modulation of at least one crack set.

Shear wave splitting occurs when a shear wave enters an anisotropic medium. The shear wave is split into approximately perpendicular fast and slow components and is akin to optical birefringence. The polarization of the fast direction (ϕ) is related to the orientation of the anisotropic symmetry axes whereas the lag time between fast and slow shear waves (δt) indicates the magnitude of the anisotropy in the ray direction. With many measurements from a range of directions one can infer the symmetry. Anisotropy can be caused by cracks with preferential alignments, by layering, or it can be intrinsic to minerals in the rock that may be aligned. In this paper the term crack is used rather loosely to mean either microcracks or macrocracks (fractures) or even preferentially aligned pore spaces.

Anisotropy due to cracks can be affected by changes in stress and pore pressure (Nur & Simmons 1969). Cracks tend to align parallel to the maximum stress direction, so that changes in the orientation of the principal stress direction will change which crack orientations are open and hence change ϕ. Changes in the magnitude of stress or pore pressure will affect the crack density and aspect ratio, and hence δt. Therefore, observing changes in δt and ϕ with time can be used to infer changes in magnitude and direction of the horizontal principal stress.

Previous measurements of shear wave splitting in tectonically active regions tend to be scattered, and temporal variations are difficult to identify. Changes in shear wave splitting in small events before and after a large earthquake in Nevada led to the suggestion that such changes could be used to predict earthquakes (Gupta 1973, see also discussion in Crampin *et al.* 1981). Changes in ϕ after the eruption of the Ruapehu volcano, New Zealand, suggested a change in principal stress direction or increase in pore pressure (Miller & Savage 2001). It has been proposed that variations in δt could be used to measure stress build up and predict earthquakes

*Current address: Atmospheric, Oceanic & Planetary Physics, Department of Physics, University of Oxford, Clarendon Laboratory, Parks Road, Oxford OX1 3PU, UK.

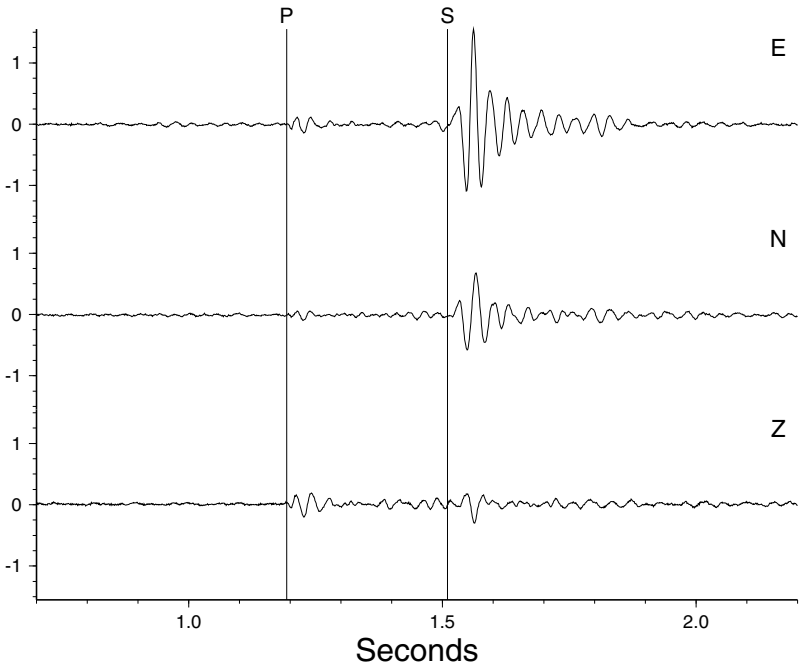

Figure 1. Example of a typical unfiltered three-component seismogram. It can be seen that the data have very low noise and clearly defined *P* and *S* waves. However, the signal is somewhat band limited due to the receiver response.

in Iceland (Crampin *et al.* 1999). An explanation for the scatter in this and other shear wave splitting studies has been proposed by Crampin *et al.* (2003). A very small decrease in δt during a borehole fluid injection experiment was interpreted in terms of stress release (Bokelmann & Harjes 2000). A gradual increase in δt was suggested in data recorded near the Anza seismic gap, California (Peacock *et al.* 1988), although the results were contentious (Aster *et al.* 1990; Crampin *et al.* 1991; Aster *et al.* 1991).

2 DATA AND GEOLOGICAL SETTING

In our study we have measured shear wave splitting from microseismic events at the Valhall oil reservoir in the North Sea. The experiment was commissioned by Amoco and conducted by ABB Offshore. Valhall is an overpressured, undersaturated Upper Cretaceous chalk reservoir. The reservoir consists of the Tor and Hod chalk formations. The overburden is siltstone with limestone stringers. Production-induced subsidence has caused many microseismic events. The located events occur mainly in the overlying siltstone cap rock. The Valhall data set presents a unique opportunity to study time-varying anisotropy because of the potentially large stress changes, continuously recorded data and the large number of events in a small region. Also the seismic data from Valhall have a very low noise level. Fig. 1 shows a typical three-component seismogram.

The microseismic data are from six three-component (ENZ) receivers situated in a well which was disused because of well-bore failure. Receivers were spaced 20 m apart in a vertical string at a depth of between 2000 and 2100 m and measured velocity with a sampling interval of 1 ms. The receivers were oriented using azimuthally varying airgun shots from a boat at 2 km offset. However, examination of the *P*-wave particle motion indicates slight misorientation of the receivers. Therefore, in this paper we have corrected for misorientations by rotating the seismograms from each receiver by the corrections given by De Meersman (2001). Receivers were labelled 1–6, with receiver 1 at the top of the string. 572 events were recorded in June and July 1998. The frequency band of the recorded events is between 20 and 80 Hz.

Events were located by Dyer & Jones (1998) using the *P*–*S* time difference to obtain the radial source–receiver distance and the *P*-wave particle motion to obtain the direction of the source. Locations were refined by iterative ray tracing through a 1-D velocity model, initially based on the well log, such that the travel time residuals were minimized. Due to the linear configuration of receivers, the source locations are most accurate in the radial direction. Location errors were typically 15–30 m depending on the geometry and noise level.

P- and *S*-wave arrivals were clear enough to locate 324 of the 572 microseismic events (Dyer & Jones 1998; Dyer *et al.* 1999; Maxwell 1999). Figs 2(a)–(c) show the locations of events that gave reliable shear wave splitting measurements in relation to the receiver string. Microseismic events were mainly clustered about 200–400 m SW of the receiver string and just above the reservoir. The typical angle of incidence of incoming rays was about 30–50° from vertical.

3 METHODS

Seismograms were rotated into the frame of the ray (radial and transverse components) to improve the clarity of the *S* wave and maximize the energy used in the analysis to provide more accurate measurements. Rotations were defined by the *P*-wave particle motion. For weakly anisotropic media the *P*-wave particle motion is polarized nearly parallel to the ray direction, so it is valid to use the particle motion as a proxy for ray direction. First a *P*-wave window was selected, which was typically 65 ms, then robust estimation (L1

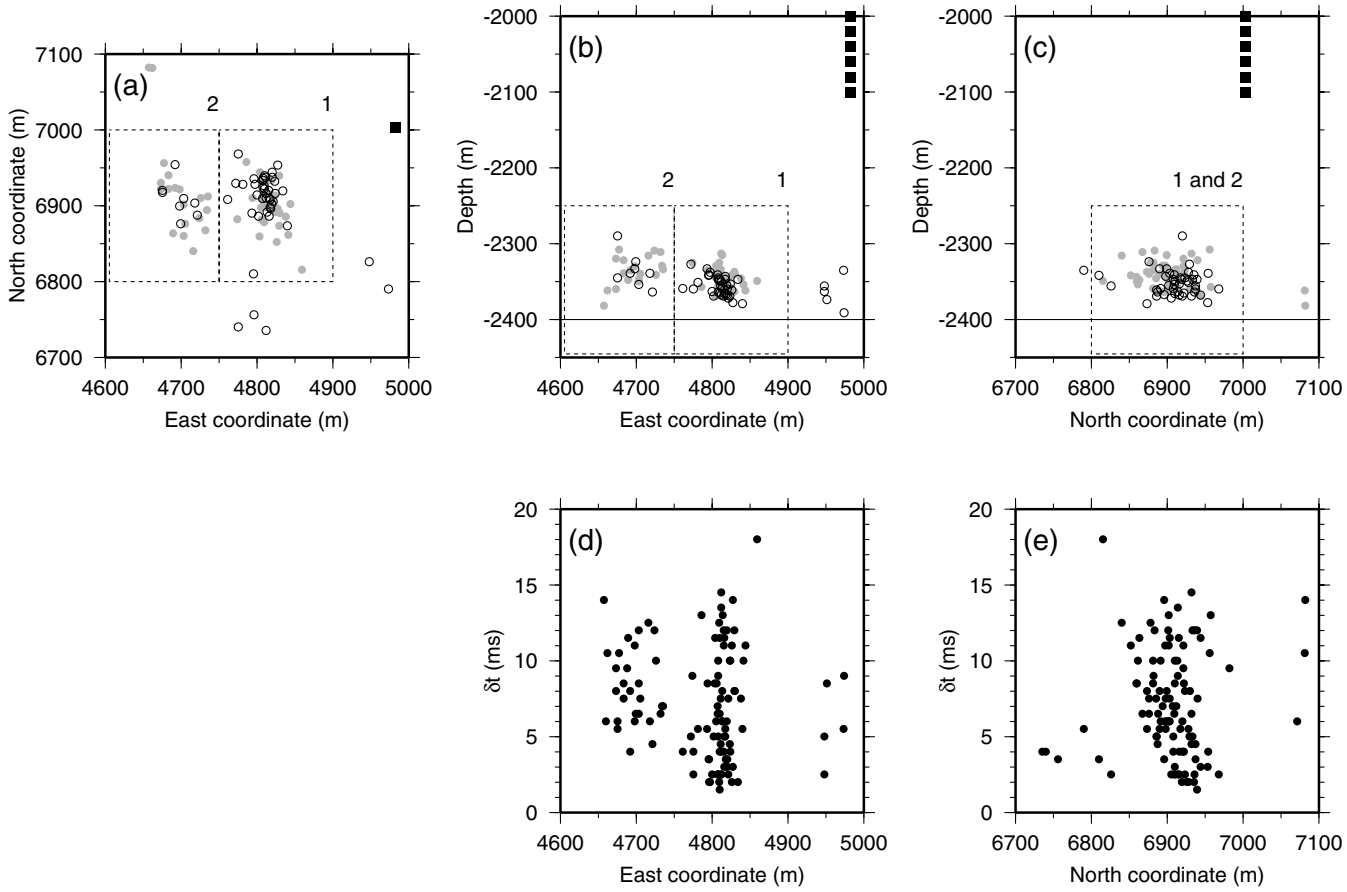

Figure 2. (a)–(c) Locations of microseismic events which gave reliable shear wave splitting measurements. Circles are event locations; solid squares are receiver locations; numbered boxes show the two main event clusters; and the solid line at −2400 m is the top of the reservoir. Solid grey circles show events which have per cent anisotropy >1 per cent and black open circles have per cent anisotropies <1 per cent. (d) and (e) show the variation of lag time δt with offset in the east and north directions. These is no systematic dependence of per cent anisotropy or δt on location.

norm) was used to find the rotation angles in the horizontal and vertical planes. Uncertainties of rotation angles were found using a bootstrap technique (Press *et al.* 1989). Alternatively, for data which were too noisy or which had poorly defined *P* waves, a linear path between source and receiver was assumed.

We applied the splitting correction method of Silver & Chan (1991) to each of the six receivers for all 324 located events. We determined δt, ϕ and the initial polarization of the *S* wave at the source using a grid search over fast directions of −90 to +90° and lags of 0–40 ms to find ϕ and δt which best linearize the *S*-wave particle motion, determined by minimizing the second eigenvalue of the particle motion covariance matrix. Measurements of anisotropy were considered reliable if: the *S* wave was well defined and distinct from the *P* wave; the fast and slow shear waves had similar waveforms; the particle motion was linearized after the correction; energy on the corrected transverse component was minimized; and the grid search gave a unique solution. A review by Savage (1999) provides an overview and examples of this splitting technique.

Because the data were band limited we sometimes experienced problems with cycle skipping in results from individual receivers. A stacking technique, first introduced by Wolfe & Silver (1998), was used to obtain a more reliable result for each event. However, some events were as close as 200 m to the receivers, so measurements of ϕ and δt at opposite ends of the 100 m string sampled a slightly different path. Stacking all six receivers would therefore lead to a blurring of the solution so we restricted our stacks to 40 m subarrays of three receivers. The results from stacking receivers 1–3 are reported here because they had the highest signal to noise ratio and steepest angles of incidence. Stacking introduced consistency of measurements for each event as an additional constraint and is therefore more robust than measurements from individual receivers. From the 324 located events, 144 reliable stacked results were obtained. Additionally, we rejected measurements that had errors greater than 15° in ϕ and 1.5 ms in δt, leaving us with 117 and 110 reliable measurements for ϕ and δt respectively. The range of δt is 0–20 ms, which, assuming an *S*-wave velocity of 600 m s^{-1} (Dyer & Jones 1998), gives a per cent anisotropy of 0–3 per cent when distributed uniformly over the ray path. These values are therefore minimum estimates of the per cent anisotropy along the ray path.

4 RESULTS

The exceptional number of high-quality splitting measurements in a short time-frame allows us to investigate temporal variations in the anisotropy. However, as shown in Figs 2(a)–(c) the events occur in two main clusters, so in order to separate path effects from temporal variations we must discuss these clusters separately.

Figs 2(a)–(c) show the per cent anisotropy as a function of location, with clusters 1 and 2 marked. Anisotropies have been split into those above and below the average value of 1 per cent. There is no obvious location-dependent trend. Figs 2(d) and (e) show δt

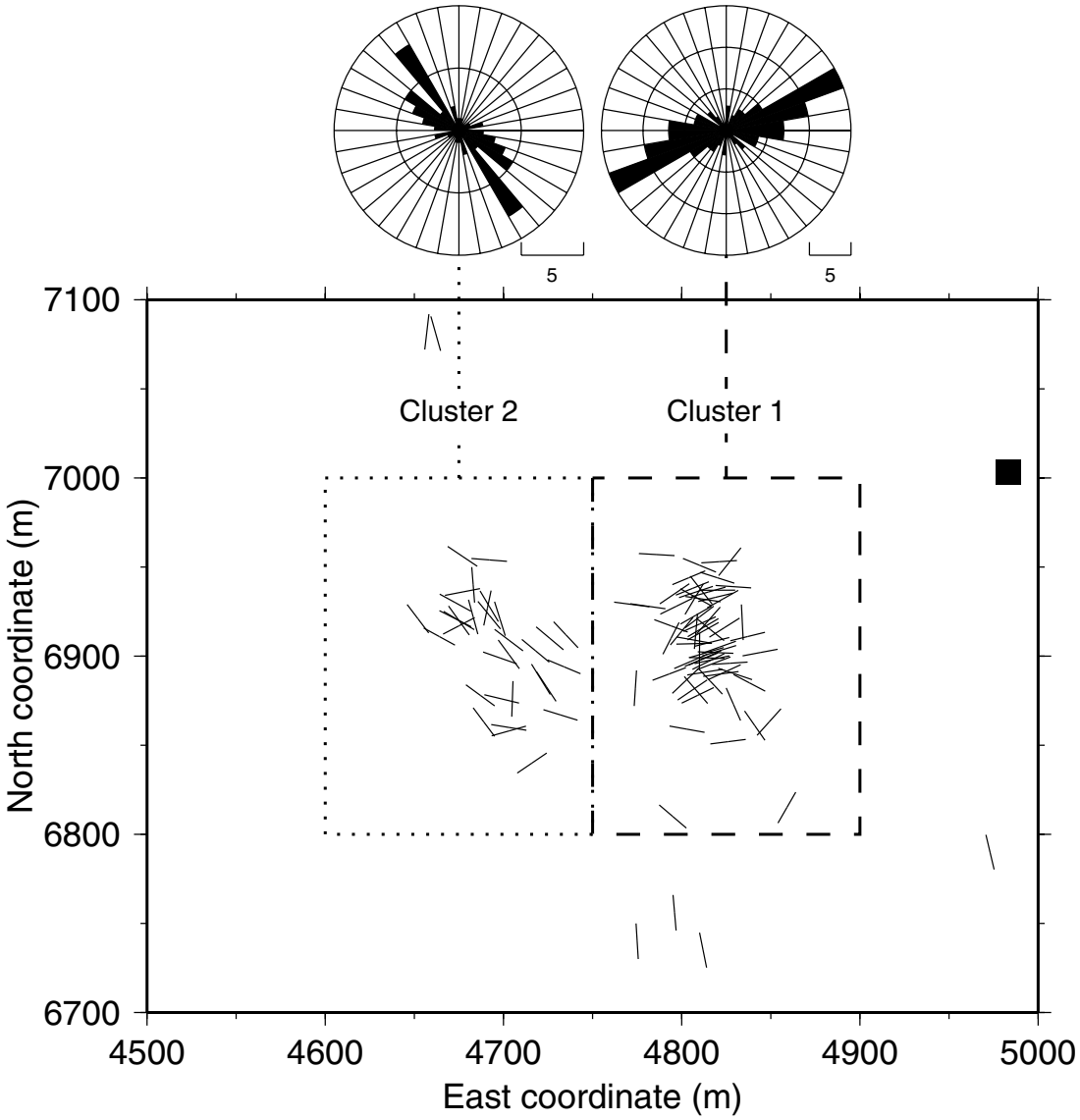

Figure 3. Map view of the orientation of fast direction strike and histograms of fast direction for each cluster. The fast direction is location dependent and exhibits a distinct distribution of values in each cluster. The black square shows the location of the receivers.

as a function of offset in the east and north directions. There is no systematic change in δt with location, implying that any temporal variations cannot be explained by path-dependent effects.

Fig. 3 shows a map of ϕ over the entire study area. There is a strong location dependence in ϕ and preferred directions of $65 \pm 5^{\circ}$E and $130 \pm 20^{\circ}$E for clusters 1 and 2 are clearly visible.

Figs 4(a)–(d) show the temporal variation of ϕ and per cent anisotropy for the two clusters (the best-fit curves to the per cent anisotropy variations are cubic B-spline fits with a knot spacing of 6 days and the error envelope is defined by the rms misfit of the data from the curve over a 6-day sliding window). The most striking feature of these plots is the very clear variation in per cent anisotropy from days 1–25 (June) visible in the Cluster 1 results. The per cent anisotropy has a low value of about 0.5 per cent around days 1 and 25, and larger anisotropies between, with values reaching over 2 per cent. This trend is also present in the Cluster 2 data, in phase with the Cluster 1 trend, although with fewer data points.

After day 25, the per cent anisotropy in Cluster 1 increases again to a value of around 2 per cent for days 30–35. After day 25 the variation of per cent anisotropy between the two clusters is possibly out of phase, although there is more scatter in the data for the last half of the experiment. To calculate the statistical significance of the temporal trends in per cent anisotropy we try to disprove the null hypothesis that the measurements are the result of random scatter. We took 10-day segments of the data and used the Kolmogorov–Smirnov test (Press *et al.* 1989) to compare the cumulative distribution function of the 10-day segments with that of the whole 60-day data set. For both clusters the null hypothesis could be rejected at the 90 per cent level.

For ϕ there are no obvious temporal trends, and separating the data into clusters 1 and 2 accounts for most of the variations. However, in Cluster 1 there is a tentative variation in ϕ at day 10, where ϕ briefly increases to around 120°E. This may be associated with the large increase in per cent anisotropy around this time, although for the rest of the experiment ϕ remains around 65°E.

We checked the robustness of the splitting measurements in a number of ways. In addition to stacking receivers 1–3, we also stacked receivers 2–4, 3–5 and 4–6 and used different criteria for

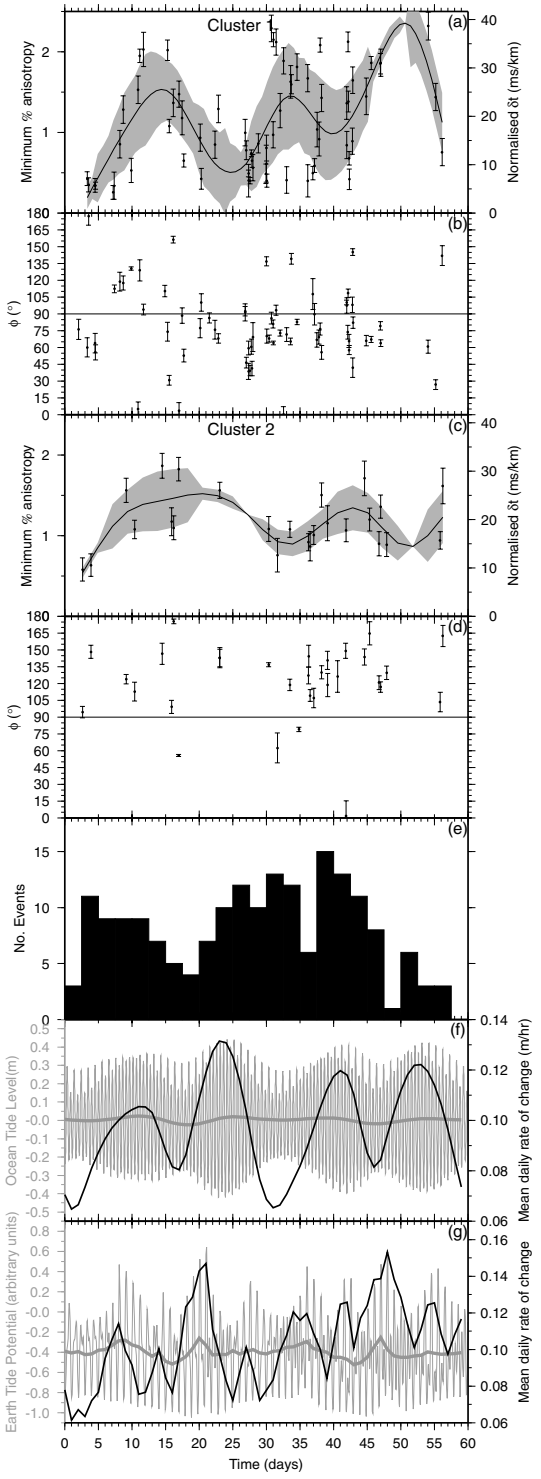

Figure 4. Variation in per cent anisotropy and polarization of the fast shear wave as a function of time for Cluster 1 (a, b) and Cluster 2 (c, d). The best-fitting curve and error envelope are shown for the per cent anisotropy. Temporal trends in the per cent anisotropy are visible. The seismicity shown in (e) also displays temporal variability. Synthetic ocean (f) and Earth (g) tides for our study area are shown, where thin grey lines are tidal signals, thick grey lines are daily means, and black lines are daily mean rates of change of tidal signal. There appears to be a superficial correlation between variations in per cent anisotropy, seismicity and tides.

maximum errors in ϕ and δt. In all cases the same patterns in ϕ and per cent anisotropy were observed, except that there was more scatter when noisier data from lower receivers were included. The temporal variation in per cent anisotropy between days 1 and 25 was especially robust. We think that some of the scatter is due to imprecise source locations as it is difficult to accurately locate sources with a single string of receivers. An error in location of 30 m for an event 300 m from the receivers would introduce an error in the per cent anisotropy of about 0.2 per cent (i.e. ± 10 per cent of the measurement), so the observed temporal variations of the order of 1 per cent are robust. We also repeated our analyses using locations derived from an alternative velocity model (Maxwell 1999). Again, the same trends were observed in ϕ and per cent anisotropy.

Fig. 5 shows specific examples of the splitting variations with time. Over an 8-week time period, high-quality splitting measurements show a variation in magnitude of a factor of three. All the events shown are within a $60 \times 60 \times 60$ m region within Cluster 1, so the differences can only be attributed to temporal variations and not path effects. We conclude that the temporal variations are real and not an artefact of location effects or scatter in the data.

5 DISCUSSION AND MODELLING

Possible causes of anisotropy at Valhall are aligned cracks, lattice-preferred orientation (LPO) of anisotropic minerals and fine-scale layering. The orientation of the fast shear wave provides information on the symmetry of the anisotropy, whereas the lag time can be used to determine the crack density, degree of LPO or layering parameters. In order to gain insight into the cause of anisotropy at Valhall we investigated various anisotropic models incorporating these possibilities. Models used the same source–receiver distances and geometries as the two main clusters at Valhall (i.e. Cluster 1, 30° incidence and 60°E ray azimuth; Cluster 2, 50° incidence and 70°E ray azimuth). Elastic constants were calculated using the effective medium theory of Schoenberg & Sayers (1995), following the approach of Hall & Kendall (2000), which allows multiple crack sets to be included. Synthetic seismograms were created using an anisotropic ray tracer (Guest & Kendall 1993) and were processed in the same way as the real data (i.e. rotation of the seismograms based on *P*-wave particle motion, followed by application of the splitting correction of Silver & Chan (1991) to calculate ϕ and δt). All models had a matrix with $V_P = 2000$ m s^{-1}, $V_S = 1000$ m s^{-1}, $\rho = 2400$ kg m^{-3}, and water-filled cracks with $V_P = 1500$ m s^{-1}, $V_S = 0.01$ m s^{-1}, $\rho = 1000$ kg m^{-3}, and aspect ratio $= 0.001$.

We first consider a single set of water-filled vertical cracks. Figs 6(a) and (b) show ϕ and δt calculated for crack strikes of 0–180°E. A crack density of 0.05 accounts for δt values of up to 20 ms observed at Valhall. However, this figure would be greater if the anisotropy was concentrated in a thin layer. Fig. 6(a) also shows that it is impossible to obtain the high values of ϕ observed in Cluster 2 with only a single set of vertical cracks. This is due to a crossover on the shear wave surfaces, where the polarity of the fast shear wave changes by 90° across the intersection singularity (Crampin & Yeldin 1981). Dipping cracks (at 10–75° from vertical) could explain the observed ϕ, but at these depths we expect vertical cracks, aligned with the vertical maximum stress direction. Additionally, seismic reflection data show dips of no more than a few degrees.

We then considered models with various combinations of cracks and layers and calculated what fast directions and lag times would be observed. Only flat layers were investigated as seismic reflection data show dips of less than a few degrees in the area. Modelling results

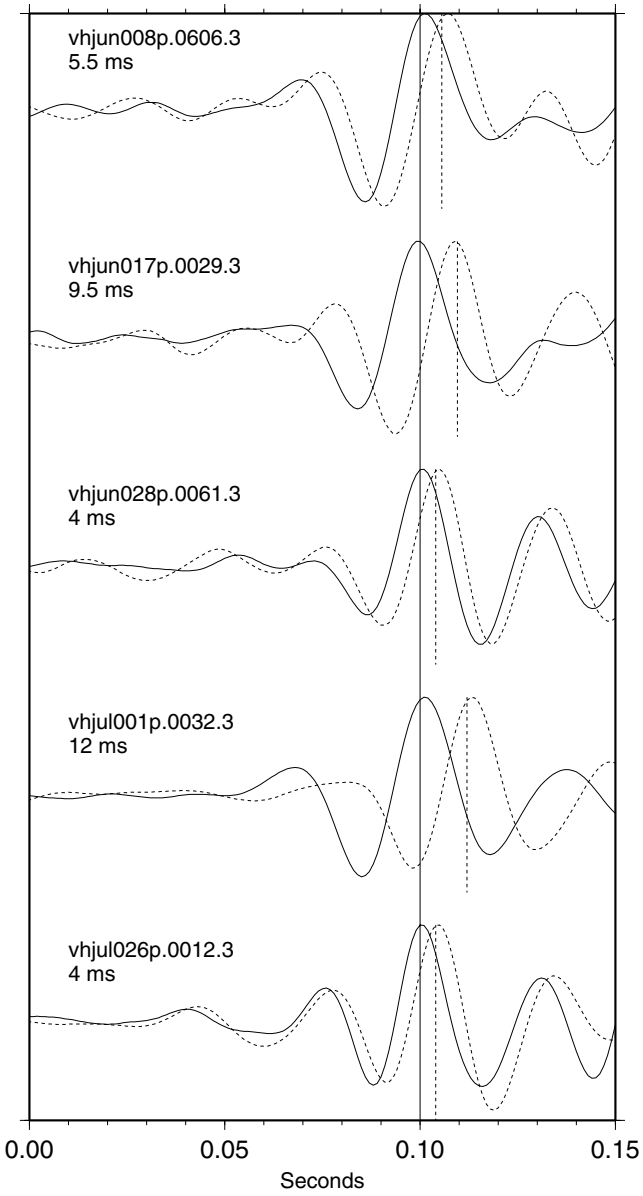

Figure 5. Example seismograms for receiver 3 projected into fast (solid line) and slow (dashed line) directions. These events have all been selected from Cluster 1 and are contained within a 60 × 60 × 60 m subcube. Measurements of δt are given under the event label, and illustrate the temporal variations in anisotropy. Seismograms have been filtered using a two-pole bandpass Butterworth filter with corner frequencies of 10 and 50 Hz. The solid vertical line is the maximum of the fast shear wave. The dashed vertical line is shifted by δt. The large variation in δt in such a small volume shows that the temporal variation is not an artefact of source location.

using anisotropic poro-elasticity (APE) theory (Crampin *et al.* 2002; Zatsepin & Crampin 1997; Crampin & Zatsepin 1997), were also examined. The scenarios which explain the observations best are:

(1) **Transverse isotropy plus cracks.** This model has a constant background anisotropy due to LPO of constituent minerals (or perhaps fine-scale layering) and a vertical crack set at 65°E. Elastic constants for the layers are from unpublished X-ray goniometry measurements on siltstone chippings from the Valhall borehole by M. Casey (University of Leeds). These results showed an intrinsic VTI (vertical transverse isotropy) symmetry due to LPO. Figs 6(c) and (d) show δt and ϕ in clusters 1 and 2 as a function of crack density for this model. To account for the observed fast directions, the crack density must be such that the cracks dominate anisotropy in Cluster 1 and the LPO dominates the anisotropy in Cluster 2. This can be used to bracket the crack density (for the parameters we used to 0.02–0.035). Increasing the crack density increases δt in Cluster 1 and decreases δt in Cluster 2. This means that for an in-phase variation in per cent anisotropy in clusters 1 and 2, as observed in Figs 4(a) and (c) for days 1–25, an increase in crack density in Cluster 1 corresponds to a decrease in crack density for Cluster 2, or vice versa. This could correspond to stress being transferred from one area to another via microseismic events. The radius of the Fresnel zone is about 50 m, so for rays from the two clusters to be affected by distinct regions of anisotropy we would expect the anisotropy to be closer to the events. For an out-of-phase variation of per cent anisotropy between clusters, as possibly observed after day 25, the crack density in the two clusters would vary in the same sense. The 65°E crack direction implies a maximum horizontal stress direction NE–SW. In this model the temporal variations in per cent anisotropy are caused by changes in stress or pore pressure changing the crack density.

(2) **Network of stress aligned microcracks** with high pore pressure. We examined the results of modelling a network of vertical cracks at high pore pressure using anisotropic poro-elasticity (APE) theory (Crampin *et al.* 2002). At high pore pressure the fast direction changes by 90° relative to the usual low pore pressure case. Cracks are open parallel to the maximum horizontal stress as usual; however, the high pore pressure allows low-aspect-ratio cracks perpendicular to the maximum horizontal stress to open. This changes the symmetry of the anisotropy such that the fast shear wave is oriented perpendicular to the maximum horizontal stress for angles of incidence of less than ≈35°, ($\Rightarrow \phi = 60°$ in Cluster 1), and the fast shear wave is oriented parallel to the maximum horizontal stress for angles of incidence of over ≈35° ($\Rightarrow \phi = 160°$ in Cluster 2) (see Fig. 4 in Crampin *et al.* 2002). The maximum horizontal stress direction would be NW–SE and the pore pressure would have to be high enough to open cracks perpendicular to this direction. If pore pressure were critically high (i.e. comparable to the confining stress), the network of microcracks would be sensitive to small changes in stress or pore pressure, which could explain some of the scatter in our data (Crampin *et al.* 2003). In this model the temporal variations in per cent anisotropy are caused by changes in stress or pore pressure changing the aspect ratio of microcracks.

Because of the limited azimuth range of our observations it is not possible to distinguish between these models based solely on the shear wave splitting results. To further constrain our interpretations we test the consistency of our observations and models with independent evidence from the Valhall region. A study of *P*–*S* converted wave amplitudes from an ocean bottom seismic survey of the Valhall field found principal symmetry directions of anisotropy to be oriented NE–SW and NW–SE (Granger *et al.* 2000). Results from a separate study of *P*-wave amplitude variation with offset and azimuth (AVOA) also exhibit this symmetry (Hall & Kendall 2003). These orientations are consistent with our fast directions and suggest cracks as the cause of anisotropy. Also we would expect cracks to be present, as the very fact that microseismic events occur indicates brittle failure. The observations of converted wave amplitudes and AVOA are consistent with both of our proposed models.

A map of regional stress (Reinecker *et al.* 2003) obtained from borehole breakouts shows a maximum horizontal stress direction NW–SE. However, a composite fault plane solution (Zoback & Zinke 2002) from the Valhall data set implies normal faulting with

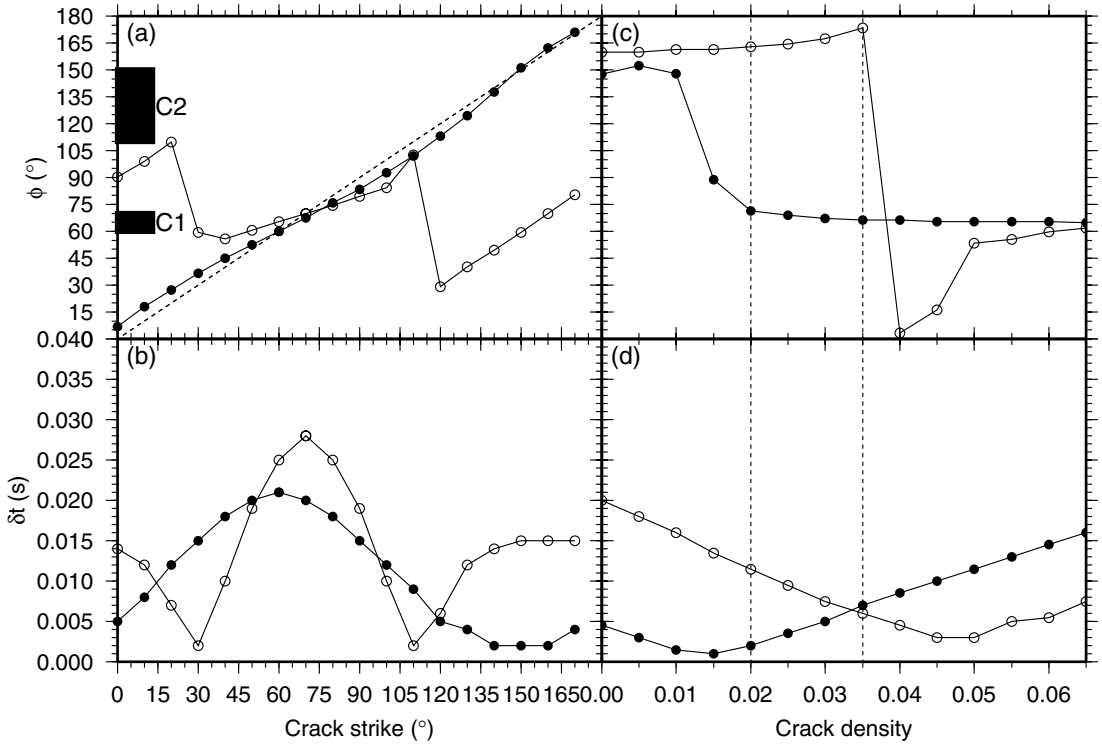

Figure 6. Modelling results. Solid circles show results for Cluster 1 geometry (angle of incidence 30° from vertical and receiver azimuth 60°E) and open circles show results for Cluster 2 geometry (angle of incidence 50° and receiver azimuth 70°E). Thick lines labelled C1 and C2 show the observed ϕ for clusters 1 and 2 for comparison. (a, b) A single set of vertical cracks with strikes from 0–180°. A crack strike of 65°E can explain $\phi = 65 \pm 5$°E as observed in Cluster 1. However, it is not possible to explain $\phi = 130 \pm 20$°E as observed in Cluster 2 using a single set of vertical cracks. (c, d) A VTI background model (from X-ray goniometry measurements on siltstone chippings) with a set of vertical cracks at 60°E with crack density varying from 0 to 0.065. This configuration can explain $\phi = 65$°E in Cluster 1 and $\phi = 130$°E in Cluster 2 if the crack density is in the range 0.02–0.035 (represented by vertical lines in (c) and (d)). In this range anisotropy is dominated by cracks in Cluster 1 and layers in Cluster 2. Note that δt in the two clusters changes in an opposite sense as crack density is increased.

tension NW–SE. The disagreement may be due to local stress variations. Model 2 is consistent with the regional stress map and Model 1 is consistent with the fault plane solution, although both the fault plane solution and regional stress are poorly constrained. To further constrain the cause of anisotropy would require measurements from additional boreholes over a greater range of azimuths.

In all models, temporal variations in anisotropy are caused by variations in stress or pore pressure modulating the density or aspect ratio of cracks. Possible sources of stress or pore pressure variations are Earth and ocean tides, and oil-production processes. The monthly variation of per cent anisotropy observed in Cluster 1 suggests tides as a possible source. Yamamura *et al.* (2003) found a strong correlation between the tidal signal and *P*-wave velocity in a year-long time-series, which they interpret as tidal modulation of pore space. This indicates that it is possible for tides to affect seismic properties. Our anisotropy measurements are at a depth of around 2 km, so we would expect some low-pass filtering of tidal signals by the overlying viscoelastic rock mass. Therefore, long-period tidal variations should have more effect than short-term fluctuations. The rate of change of tidal load could also be important, as discussed by Yamamura *et al.* (2003).

Fig. 4 compares the per cent anisotropy in each cluster with seismicity, synthetic ocean tide level calculated from tidal model NAO99 (Matsumoto *et al.* 2000) and synthetic Earth tide potential calculated using the model of Chang & Firoozabadi (2000). The daily mean tide level and daily mean rate of change of tide level are also shown. The range of variation in daily mean tidal signals is very small, suggesting that either the envelope/range or rate of change of tidal load has a greater effect on crack properties. Interestingly, the peaks and troughs in per cent anisotropy seem to be approximately aligned with maximum (spring) and minimum (neap) tidal variations. This, along with the occurrence of monthly periods in the per cent anisotropy and seismicity, suggests a link between tides, crack properties and pore pressure or stress.

The exact mechanism by which tides affect crack properties is not clear at this stage. It is possible that tides modulate pore pressure/stress at depth, which could affect cracks directly. Alternatively, small changes in pore pressure/stress could cause microearthquakes, resulting in a larger change in pore pressure/stress and a corresponding change in crack properties. However, as our time-series are only 60 days long the correlation of tides and per cent anisotropy may be a coincidence and a longer study period would be required for conclusive proof of tidal modulation.

The correlation of per cent anisotropy and seismicity might be expected, as when a microseismic event occurs stress is released, which will affect crack properties. Oil production and subsequent re-stressing of the reservoir could be another modulating effect on our measurements. Oil-field activities have previously been observed by Angerer *et al.* (2002) to affect shear wave splitting.

6 CONCLUSIONS

Over 100 reliable measurements of ϕ and δt, combined with the use of modelling, have allowed the origin of anisotropy in the Valhall

region to be constrained to either (1) LPO-induced transverse isotropy plus vertical cracks or (2) a network of stress-aligned microcracks. The most important result of this study is the clear measurement of time-variant shear wave splitting. This shows that it is possible to monitor changes in crack properties induced by changes in pore pressure or stress.

A possible explanation for the temporal variation is that stress, and hence cracks, is modulated by tidal loading. An apparent correlation of tidal variation and per cent anisotropy support this suggestion, although a longer time-series is required for conclusive proof. Another possible explanation is that oil production in the area causes changes in stress or pore pressure, which in turn affects crack properties. In future, multiple receiver locations and longer time-series will enable more detailed interpretations to be drawn.

ACKNOWLEDGMENTS

This work was supported by ABB Offshore Systems, BP Norge, Shell Exploration and Production UK, Schlumberger Cambridge Research and NERC. Microseismic data were provided by ABB and BP. We thank Tilo Schoene at GFZ-Potsdam for the NAO99 synthetic ocean tide series. We also thank Stuart Crampin and Martha Savage for insightful reviews, which improved the manuscript. The views in this paper are those of the authors and not necessarily those of the organizations for which they work.

REFERENCES

Angerer, E., Crampin, S., Li, X. & Davis, T.L., 2002. Processing, modelling and predicting time-lapse effects of overpressured fluid-injection in a fractured reservoir, *Geophys. J. Int.,* **149,** 267–280.

Aster, R.C., Shearer, P.M. & Berger, J., 1990. Quantitative measurements of shear-wave polarizations at the Anza seismic network, Southern California—implications for shear-wave splitting and earthquake prediction, *J. geophys. Res.,* **95,** 12 449–12 473.

Aster, R.C., Shearer, P.M. & Berger, J., 1991. Comment on quantitative measurements of shear-wave polarizations at the Anza seismic network, Southern California—implications for shear-wave splitting and earthquake prediction by Aster, Richard, C., Shearer, Peter, M., Berger, Jon—Reply, *J. geophys. Res.,* **96,** 6415–6419.

Bokelmann, G.H.R. & Harjes, H.P., 2000. Evidence for temporal variation of seismic velocity within the upper continental crust, *J. geophys. Res.,* **105,** 23 879–23 894.

Chang, E. & Firoozabadi, A., 2000. Gravitational potential variations of the Sun and Moon for estimation of reservoir compressibility, *Soc. Petrol. Eng. J.,* **5,** 456–465.

Crampin, S. & Yeldin, M., 1981. Shear-wave singularities of wave-propagation in anisotropic media, *J. Geophys.,* **49,** 43–46.

Crampin, S. & Zatsepin, S.V., 1997. Modelling the compliance of crustal rock–II. Response to temporal changes before earthquakes, *Geophys. J. Int.,* **129,** 495–506.

Crampin, S., Evans, R., Doyle, M. & Davis, J.P., 1981. Comments on papers about shear-wave splitting in dilatancy-induced anisotropy by I. N. Gupta, A. Ryall, & W. U. Savage, *Bull. seism. Soc. Am.,* **71,** 375–377.

Crampin, S., Booth, D.C., Evans, R., Peacock, S. & Fletcher, J.B., 1991. Comment on quantitative measurements of shear-wave polarizations at the Anza seismic network, Southern California—implications for shear-wave splitting and earthquake prediction by Aster, Richard, C., Shearer, Peter, M., Berger, Jon, *J. geophys. Res.,* **96,** 6403–6414.

Crampin, S., Volti, T. & Stefánsson, R., 1999. A successfully stress-forecast earthquake, *Geophys. J. Int.,* **138,** F1–F5.

Crampin, S., Volti, T., Chastin, S., Gudmundsson, A. & Stefánsson, R., 2002. Indication of high pore-pressures in a seismically-active fault zone, *Geophys. J. Int.,* **151,** F1–F5.

Crampin, S., Peacock, S., Gao, Y. & Chastin, S., 2004. The scatter of time-delays in shear-wave splitting above small earthquakes, *Geophys. J. Int.*, **156,** 39–44.

De Meersman, K., 2001. Improving microseismic event locations: an experiment at Valhall, *Master's thesis*, The University of Leeds, Leeds, United Kingdom.

Dyer, B.C. & Jones, R.H., 1998. 3D processing and interpretation of the microseismic data recorded during June and July 1998 in the Valhall field, *Report for Amoco by CSMA Ltd. Cornwall*.

Dyer, B.C., Jones, R.H., Cowles, J.F., Barkved, O. & Folstad, P.G., 1999. Microseismic survey of a North Sea reservoir, *World Oil,* **220,** 74–78.

Granger, P.-Y., Rollet, A. & Bonnot, J.-M., 2000. First evaluation of azimuthal anisotropy over Valhall field, in *Anisotropy 2000: Fractures, Converted Waves, and Case Studies*, pp. 49–68, eds Ikelle, L. & Gangi, A., Society of Exploration Geophysics, Tulsa, USA.

Guest, W.S. & Kendall, J.M., 1993. Modelling seismic waveforms in anisotropic inhomogeneous media using ray and Maslov asymptotic theory: applications to exploration seismology, *Can. J. Expl. Geophys.,* **29**(1), 78–92.

Gupta, I.N., 1973. Premonitory variations in *S*-wave velocity anisotropy before earthquakes in Nevada, *Science,* **182,** 1129–1132.

Hall, S. & Kendall, J.-M., 2000. Constraining the interpretation of AVOA for fracture characterisation, in *Anisotropy 2000: Fractures, Converted Waves, and Case Studies*, pp. 107–144, eds Ikelle, L. & Gangi, A., Society of Exploration Geophysics, Tulsa, USA.

Hall, S. & Kendall, J.-M., 2003. Fracture characterisation at Valhall: application of *P*-wave AVOA analysis to a 3D ocean-bottom data set, *Geophysics*, **68,** 1150–1160.

Matsumoto, K., Takanezawa, T. & Ooe, M., 2000. Ocean tide models developed by assimilating TOPEX/POSEIDON altimeter data into hydrodynamical model: a global model and a regional model around Japan, *J. Oceanogr.,* **56,** 567–581.

Maxwell, S., 1999. Relocation of Valhall microseismicity, Tech. Rep. AMOC002, ESG Report to BP-Amoco.

Miller, V. & Savage, M., 2001. Changes in seismic anisotropy after volcanic eruptions: evidence from Mount Ruapehu, *Science,* **293,** 2231–2233.

Nur, A. & Simmons, G., 1969. Stress-induced velocity anisotropy in rock: an experimental study, *J. geophys. Res.,* **74,** 6667–6674.

Peacock, S., Crampin, S. & Booth, D.C., 1988. Shear wave splitting in the Anza seismic gap, southern California: temporal variations and possible precursors, *J. geophys. Res.,* **93,** 3339–3356.

Press, W.H., Flannery, B.P., Teukolsky, S.A. & Vetterling, W.T., 1989. *Numerical Recipes,* 2nd edn, Cambridge University Press, Cambridge.

Reinecker, J., Heidbach, O. & Mueller, B., 2003. The 2003 release of the world stress map, available online at www.world-stress-map.org

Savage, M.K., 1999. Seismic anisotropy and mantle deformation: what have we learned from shear wave splitting?, *Rev. Geophys.,* **37,** 65–106.

Schoenberg, M. & Sayers, C.M., 1995. Seismic anisotropy of fractured rock, *Geophysics,* **60,** 204–211.

Silver, P.G. & Chan, W.W.J., 1991. Shear-wave splitting and subcontinental mantle deformation, *J. geophys. Res.,* **96,** 16 429–16 454.

Wolfe, C.J. & Silver, P.G., 1998. Seismic anisotropy of oceanic upper mantle: shear-wave splitting methodologies and observations, *J. geophys. Res.,* **103,** 749–771.

Yamamura, K., Sano, O., Utada, H., Takei, Y., Nakao, S. & Fukao, Y., 2003. Long-term observation of *in situ* seismic velocity and attenuation, *J. geophys. Res.,* **108,** 2317–2331.

Zatsepin, S.V. & Crampin, S., 1997. Modelling the compliance of crustal rock–I. Response of shear-wave splitting to differential stress, *Geophys. J. Int.,* **129,** 477–494.

Zoback, M.D. & Zinke, J.C., 2002. Production-induced normal faulting in the Valhall and Ekofisk oil fields, *Pure appl. Geophys.,* **159,** 403–420.